European Radiology (2019) 29:5700–5708
https://doi.org/10.1007/s00330-019-06132-9

MUSCULOSKELETAL

# Whole-body MRI vs bone scintigraphy in the staging of Ewing sarcoma of bone: a 12-year single-institution review

Sarah Kalus[1] · Asif Saifuddin[1]

Received: 16 October 2018 / Revised: 14 February 2019 / Accepted: 6 March 2019 / Published online: 26 March 2019


## Abstract

**Objective** To compare whole-body MRI (WB-MRI) at 1.5/3T and bone scintigraphy in the skeletal staging of Ewing sarcoma (ES) of bone.

**Methods** All patients with a histological diagnosis of ES of bone between 2007 and 2018 were retrospectively reviewed. The analysis included gender, mean age, skeletal distribution, and prevalence of skeletal metastases on WB-MRI and bone scintigraphy.

**Results** The study group comprised 182 patients with a mean age of 18.0 years (range 2–56 years), 126 males and 56 females. Skeletal metastases were detected overall in 30 patients (16.5%), in 23 of 96 patients (24%) who underwent WB-MRI, and in 20 of 118 patients (16.9%) who underwent bone scintigraphy. Of 71 patients who underwent both WB-MRI and bone scintigraphy, skeletal metastases were detected on both modalities in 13 (18.3%), while in 4 patients, skeletal metastases were identified on WB-MRI alone. There were no patients in whom skeletal metastases were identified on bone scintigraphy alone. Of 13 patients with skeletal metastases who underwent both studies, WB-MRI showed a greater number of metastatic foci in 10 (76.9%). However, scintigraphy was superior to WB-MRI in detecting skull vault lesions, but did show false-positive results around the long bone growth plates.

**Conclusion** WB-MRI is more sensitive than bone scintigraphy in detecting skeletal metastases in ES of bone, with the exception of skull vault metastases. Consideration should be given to replacing bone scintigraphy with WB-MRI.

**Key Points**

- *Whole-body MRI is more sensitive than bone scintigraphy in detecting skeletal metastases in Ewing sarcoma of bone.*
- *Whole-body MRI can safely replace bone scintigraphy for staging of the skeleton, with the acknowledgement of the possibility of missing a clinically occult skull vault metastasis.*

**Keywords** Ewing sarcoma · Magnetic resonance imaging · Radionuclide imaging

**Abbreviations**

| | |
|---|---|
| ES | Ewing sarcoma |
| OS | Osteosarcoma |
| WB-MRI | Whole-body MRI |

## Introduction

Ewing sacrcoma (ES) is the second commonest primary bone malignancy in children and adolescents, after osteosarcoma (OS) [1–3]. Accounting for 3% of all paediatric cancers, ES has an incidence of approximately 3 per million per year [2, 3], and a peak incidence in adolescents and young adults with a median age at diagnosis of 15 years [4]. A slight male predilection (M:F ratio 1.5:1) is observed, as is a strikingly lower incidence in patients of African and Chinese descent [2–4].

All patients with a possible diagnosis of ES should be referred urgently to a specialist sarcoma centre for multidisciplinary team (MDT) discussion. As laid out in the

✉ Sarah Kalus
sarahkalus@gmail.com

[1] The Royal National Orthopaedic Hospital, Brockley Hill, Stanmore HA7 4LP, UK

British Sarcoma Group 2016 guidelines by Gerrand et al, imaging evaluation should include radiographs and MRI of the local site [4]. Where ES arises in the appendicular skeleton, MRI should include the entire involved bone and adjacent joints to detect skip metastases. Staging requires a chest CT and investigation for distant bone metastases. Whole-body bone scintigraphy is recommended by both the UK [4] and European [5] guidelines for the management of bone sarcomas, although both groups recognise the potential role of whole-body MRI (WB-MRI) and PET/CT. Bone scintigraphy is also the evaluation technique used for the assessment of skeletal metastases in the Euro Ewing 2012 trial. However, several studies comparing bone scintigraphy with MRI in a variety of tumours metastasising to bone have shown WB-MRI to be more sensitive than bone scintigraphy [6–11].

The aim of this study was to compare WB-MRI and bone scintigraphy in the skeletal staging of ES of bone in the setting of a specialist bone sarcoma service.

## Methods

The study was approved by the local Research and Development Committee with a waiver for informed patient consent. All patients with a histologically confirmed diagnosis of ES of bone between January 2007 and December 2018 were identified from the pathology database. Patients presenting with recurrent ES or extra-skeletal ES were excluded.

The analysis included gender, age and skeletal distribution of the primary tumour. Imaging studies included a combination of radiography and MRI of the primary tumour, chest CT and skeletal staging with bone scintigraphy and/or WB-MRI. All imaging studies had been reported by a consultant musculoskeletal radiologist working within the setting of a specialist musculoskeletal sarcoma service and were reviewed by a musculoskeletal radiology fellow. Where there was disagreement, a final decision was made by a consultant musculoskeletal radiologist with over 24 years of experience of musculoskeletal sarcoma imaging. All cases were also reviewed following imaging studies and biopsy at the sarcoma MDT meeting.

WB-MRI was performed using either a 1.5T system (86 cases) (Philips Achieva 1.5T) or a 3T system (10 cases) (Philips Ingenia 3T). Patients were placed supine within a Q-body coil. Sequences were as follows. For 1.5T, coronal T1-weighted spin echo (T1W SE): TR = 678 ms, TE = 18 ms, matrix of 512 and 6 mm slice thickness. Short T1 inversion recovery (STIR): TR/TI = 3000/165 ms, TE = 64 ms, matrix of 512 and 6 mm slice thickness. For 3T, coronal T1W SE: TR = 683 ms, TE = 8 ms, matrix of 512 and 6 mm slice thickness. STIR: TR/TI = 8100/230 ms, TE = 70 ms, matrix of 512 and 6 mm slice thickness. The WB-MRI examination took 30 min and was performed under general anaesthesia in young children. Skeletal metastases were diagnosed on WB-MRI if there was a single or multifocal areas of marrow abnormality on T1W SE and STIR images that had features consistent with marrow infiltration, as have been previously described in the literature (Fig. 1) [12–14].

Standard skeletal scintigraphy was performed using a planar single-phase technique. Whole-body scans were obtained 3–4 h after intravenous injection of 600 MBq $^{99m}$Tc–MDP in adults. In children, the dose was adjusted to body weight according to the ARSAC guidelines together with physicist input. Images were acquired using a dual-head gamma camera (Philips Axis Dual Head Nuclear Gamma Camera) with a low energy, high-resolution parallel hole collimator at a speed of 8.75 cm/min. The effective dose for the whole-body bone scan in adults was 2.9 mSv and the examination duration was 25 min. In some cases, the bone scan had been performed externally, but underwent the same method of review. With regard to bone scintigraphy, a skeletal metastasis was defined as focal increased radionuclide uptake relative to adjacent normal marrow, not in a location attributable to physiologically increased uptake such as the open physis, or characteristic of degenerative change (Fig. 2) [13].

For patients in whom both imaging techniques were performed ($n = 71$), the mean time interval between WB-MRI and bone scintigraphy was 2.6 days (range 0–35 days). In 41 cases (57.7%), both investigations were performed on the same day, in 64 cases (90.1%) within 1 week of each other, in 67 cases (94.4%) within 2 weeks of each other, and in 4 cases greater than 2 weeks. Twenty-eight of 118 (23.7%) nuclear medicine studies had been performed prior to referral, while 90 (76.3%) were performed at our institution.

## Results

The study group comprised 182 patients with a mean age of 18.0 years (range 2–56 years), with 126 (69.2%) males and 56 (30.8%) females. Primary tumours arose in the appendicular skeleton in 84 cases (46.2%), the flat bones in 73 (40.1%), the spine in 18 (9.9%), and the foot in 6 (3.3%). In a single case, the primary site could not be determined, the patient presenting with widespread bone lesions. The skeletal distribution of ES is summarised in Table 1. In the appendicular skeleton, tumours were found most commonly in the diaphysis (34 patients) followed by the metadiaphysis (31 patients). Twenty tumours arose in the metaphysis, of which five extended into the epiphysis. One hundred seventy-three tumours were located in the medulla, while nine arose from the surface of the bone.

Overall, 30 of the 182 patients (16.5%) had skeletal metastases on imaging, including distant metastases and skip metastases in appendicular bones. Skeletal metastases were demonstrated in 23 of the 96 patients (24%) who underwent WB-


**Fig. 1** Coronal T1W SE (**a**) and coronal STIR (**b**) whole-body MRI in a 32-year-old male with primary Ewing sarcoma of the right 5th rib (arrows) and metastases in L4, the right acetabulum, the right proximal femur, and the left ilium (arrowheads)

MRI. Of the 118 patients in whom bone scintigraphy was performed, skeletal metastases were detected in 20 (16.9%). Of the 71 patients who underwent both WB-MRI and bone scintigraphy, skeletal metastases were detected on both modalities in 13 (18.3%), while skeletal metastases were apparent on WB-MRI only in 4 patients. There were no patients who underwent both modalities in whom skeletal metastases were identified on bone scintigraphy alone. In these 13 patients, WB-MRI demonstrated a greater burden of skeletal metastatic disease in 10 (76.9%) (Figs. 1 and 2), while scintigraphy was false-positive for metastatic disease in 2 patients at the proximal humerus, the proximal femora and around the sacroiliac joints. In 7 patients where scintigraphy clearly demonstrated skull vault lesions, WB-MRI was either considered to be normal in this location or did not clearly identify the lesions in 5 cases.

Figures 3, 4, and 5 illustrate 3 of the cases in which skeletal metastases were detected on WB-MRI only. Histological confirmation of skeletal metastasis was obtained in one patient with a primary tumour in the left fifth metatarsal, who


**Fig. 2** Whole-body bone scintigraphy in the same 32-year-old male as in Fig. 1 with primary Ewing sarcoma of the right 5th rib (arrow) showing a metastasis in the right ischium (arrowhead). Note that the additional bone metastases shown on whole-body MRI in Fig. 1 are scintigraphically occult

underwent CT-guided biopsy of a left tibial lesion, confirming the diagnosis of metastatic ES (Fig. 3).

## Discussion

Accurate staging of ES is critical to establish the prognosis and to optimise treatment. Metastatic disease is reported in 26% of patients at presentation, occurring to the lungs (10%), bone/bone marrow (10%), and rarely other sites (6%) [4]. The presence of metastatic disease is the most significant adverse prognostic factor [2, 15]. In patients with ES of bone, greater survival is observed in patients with lung metastases only, compared with those with skeletal metastases or a combination of both [15]. Using current multimodality treatment including surgery, radiotherapy and chemotherapy, 5-year survival for ES is 60–70% for localised disease, but only 20–40% in patients with metastatic disease [4].

$^{99m}$Tc–MDP bone scintigraphy is currently the recommended method for staging bone sarcomas [4, 5] and is also currently the technique utilised in the Euro Ewing 2012 trial. Bone scintigraphy is more sensitive than radiography and CT for the detection of bone metastases [6, 8] and is readily available and easily performed at relatively low cost. $^{99m}$Tc–MDP

**Table 1** Skeletal distribution of primary Ewing sarcoma of bone

| Location 1 | Location 2 |
|---|---|
| Appendicular = 84 (46.2%) | Humerus = 12 (6.6%) |
| | Radius = 1 (0.5%) |
| | Femur = 41 (22.5%) |
| | Tibia = 12 (6.6%) |
| | Fibula = 18 (9.9%) |
| Pelvis = 42 (23.1%) | Ilium = 26 (14.3%) |
| | SPR = 10 (5.5%) |
| | IPR = 4 (2.2%) |
| | Ischium = 2 (1.1%) |
| Chest wall = 31 (17.0%) | Rib = 16 (8.8%) |
| | Scapula = 11 (6.0%) |
| | Clavicle = 4 (2.2%) |
| Spine = 18 (9.9%) | Mobile = 7 (3.8%) |
| | Sacrum = 11 (6.0%) |
| Foot = 6 (3.3%) | Tarsal = 2 (1.1%) |
| | Metatarsal = 4 (2.2%) |
| Other = 1 (0.5%) | Unknown = 1 (0.5%) |
| Total | 182 (100%) |

analogues localise to phosphorus groups of calcium hydroxyapatite produced by osteoblasts, and therefore uptake relies on an osteoblastic host reaction to tumour deposits, rendering it an indirect tumour marker [16]. As a result, bone metastases are detected on scintigraphy at a relatively advanced stage of tumour infiltration [7]. In contrast, MRI and FDG PET have the advantage of depicting bone metastases at an earlier stage of growth once tumour cells have deposited in the intramedullary compartment, resulting in replacement of normal haematopoietic marrow and tumour cell proliferation before the osteoblastic host reaction has occurred [7]. MRI demonstrates bone metastases with high anatomic detail as neoplastic infiltration disrupts normal bone marrow cell composition which in turn causes abnormal signal intensity, whereas FDG PET depicts the increased glucose metabolism [7].

The clinical utility of WB-MRI in detecting skeletal metastases and its superiority to bone scintigraphy have been demonstrated in a variety of tumours that metastasise to bone in both adults and children [8, 16–25]. The current study is the largest report comparing WB-MRI and bone scintigraphy in the skeletal staging of ES of bone, with the incidence of bone metastases on WB-MRI being 24% compared with 16.9% for bone scintigraphy. Also, of the 71 patients who underwent both imaging modalities, 4 had skeletal metastases detected only on WB-MRI while there were none in whom skeletal metastases were identified on bone scintigraphy alone. However, scintigraphy was clearly superior to WB-MRI in the detection of skull vault lesions, although in none of these


**Fig. 3** **a** Whole-body bone scintigraphy in an 18-year-old male demonstrates increased uptake in the left foot corresponding to the primary Ewing sarcoma in the 5th metatarsal, with no other abnormal uptake identified. Coronal T1W SE (**b**) and coronal STIR (**c**) whole-body MR images acquired on the same day show a small lesion in the left lateral tibial plateau (arrows) which was felt to be indeterminate but concerning for a metastasis. **d** CT demonstrated a small lytic lesion (arrow), which was sampled by CT-guided biopsy yielding a histological diagnosis of metastatic Ewing sarcoma (**e**)

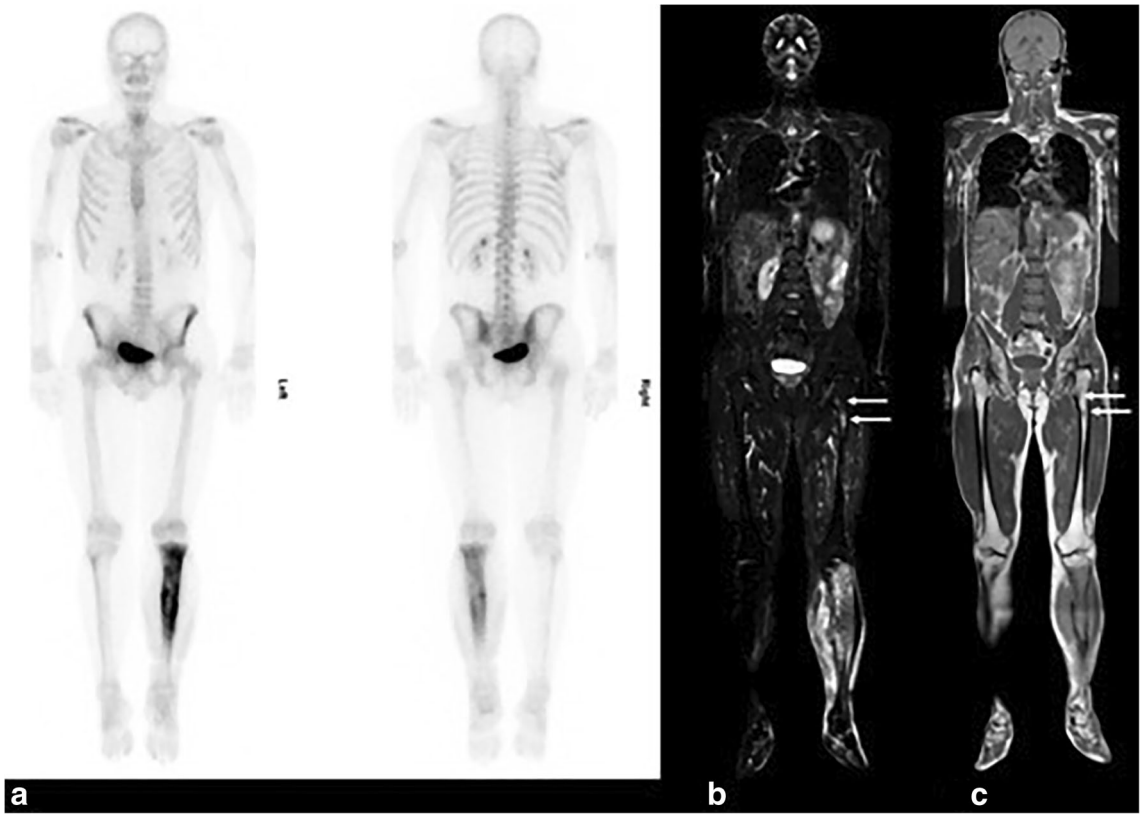


**Fig. 4** **a** Whole-body bone scintigraphy in a 43-year-old male demonstrates increased uptake in the left tibia corresponding to the primary Ewing sarcoma, with no other abnormal uptake identified. Coronal STIR (**b**) and coronal T1W SE (**c**) whole-body MR images acquired 5 weeks later demonstrate multiple focal lesions in the left lesser trochanter and proximal femoral shaft (arrows) consistent with metastases

cases were the skull vault metastases isolated. Therefore, in this group of patients, bone scintigraphy added no diagnostic value when WB-MRI was performed, which is consistent with previously reported smaller studies [7, 8, 26].

In a report of 39 children and young adults with primary tumours having the potential to metastasise to bone, including 20 with ES, Daldrup-Link et al found WB-MRI to be more sensitive than bone scintigraphy, while FDG PET was the most sensitive technique overall [7]. The reported sensitivities were 90% for PET, 82% for WB-MRI and 71% for bone scintigraphy, but with regard to ES, the sensitivities were 88% for PET and 80% for both WB-MRI and bone scintigraphy. Most false-negative results were located in the small or flat bones for MRI, in the spine for bone scintigraphy, and in the skull for PET. Daldrup-Link et al identified most false-positive findings with PET. The sensitivities of bone scintigraphy and MRI were significantly increased by either combining with each other (90%) or combining with PET (96%). However, the sensitivity of PET was not increased by the combination with either of the other imaging modalities [7]. The WB-MRI protocol used by Daldrup-Link et al constituted axial T1W SE images in all patients, with STIR acquired only in their first 10 cases. Our WB-MRI protocol comprised coronal T1W SE and STIR imaging in all cases, which may explain the increased sensitivity of WB-MRI compared with bone scintigraphy in our study, which was not found by Daldrup-Link [7].

Quartuccio et al compared the diagnostic performance of FDG PET/CT and conventional imaging, including MRI, bone scintigraphy and CT for staging and follow-up of paediatric skeletal ES and OS [26]. A total of 20 metastatic bone lesions were found in 44 patients with ES. MRI had a sensitivity of 100%, specificity of 75% and overall diagnostic accuracy of 88.9%. PET/CT had a sensitivity of 100%, specificity of only 25% and diagnostic accuracy of 85%, while bone scintigraphy had a sensitivity of 62.5%, specificity of 100% and diagnostic accuracy of 70%.

Kumar et al compared WB-MRI with skeletal scintigraphy and FDG PET in 26 paediatric patients with small round cell neoplasms, including 11 ES/PNET [8]. They found WB-MRI to have a sensitivity of 97.5%, specificity of 99.4%, positive predictive value of 97.5% and negative predictive value of 99.4%, compared with respective values of 30%, 99.4%, 92.3% and 85.6% for skeletal scintigraphy. FDG PET/CT had a sensitivity of 90%, specificity of 100%, positive predictive value of 100% and negative predictive value of 97.7% [8]. In a systematic review by Smets et al evaluating the diagnostic performance of WB-MRI in the detection of skeletal

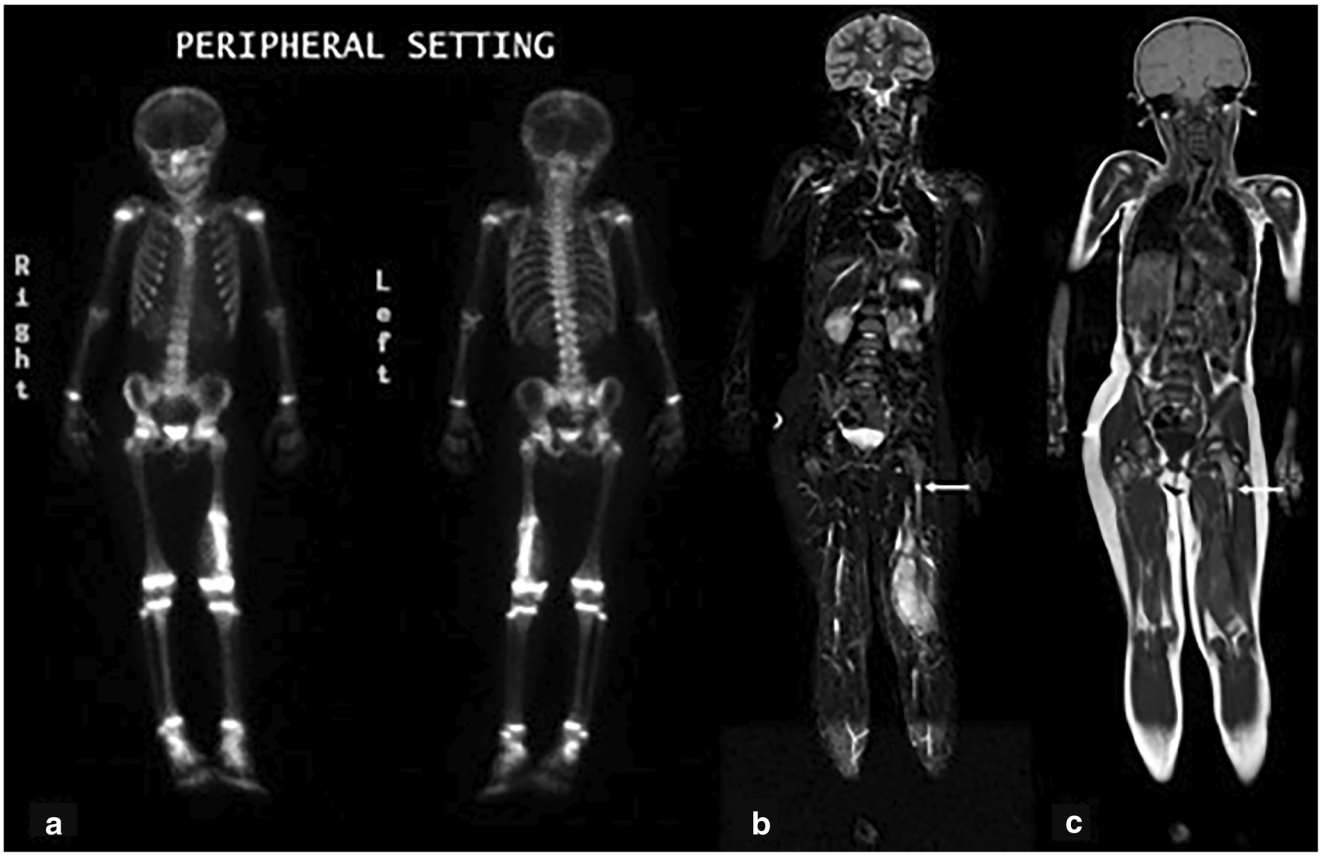


**Fig. 5** **a** Whole-body bone scintigraphy in a 5-year-old female demonstrates increased uptake in the left femur consistent with the primary Ewing sarcoma. Coronal STIR (**b**) and coronal T1W SE (**c**) whole-body MR images acquired 9 days later demonstrate a focal lesion in the left proximal femoral shaft (arrows) consistent with a skip metastasis, which was scintigraphically occult

metastases in children with malignant primary solid tumours, including 39 ES/PNET, the sensitivity of WB-MRI ranged from 82.4–100% [17].

Primary ES of bone typically has a lytic appearance, although rarely can be sclerotic [27]. In a study comparing bone scintigraphy and FDG PET/CT in staging ES, Ulaner et al examined 47 patients with ES of bone, among whom 44 primary tumours had a lytic appearance on CT while 3 were sclerotic [27]. Twelve patients had skeletal metastases, which were identified on PET/CT in 11 cases and on bone scintigraphy in 9. Ulaner et al found no additional benefit of bone scintigraphy over PET/CT in patients whose primary tumour had a lytic appearance. They suggested that bone scintigraphy may be omitted from the initial staging of ES of bone, unless rarely the primary tumour was sclerotic, as blastic metastases show low FDG uptake but are detectable on bone scintigraphy [27].

Although we did not evaluate FDG PET, its merits and drawbacks warrant some comment given its increasing use. Histological response to neoadjuvant chemotherapy, in particular tumour necrosis, is one of the most important prognostic factors in ES [28, 29]. FDG PET has been found to be accurate in assessing histological response to chemotherapy and predicting survival and is superior to MRI in this regard [28]. In a study including 45 patients with ES, Palmerini et al reported an association between standardised uptake values (SUV) at baseline and histological/radiological response in patients with ES and also found that SUV at baseline is predictive of event-free survival in ES [29]. PET also has the advantage of detecting extra-skeletal metastases which may not be apparent on MRI or bone scintigraphy. However, PET requires additional CT or MRI to overcome its poor spatial resolution and is also limited in the detection of skull metastases due to the high glucose metabolism in normal brain [7]. Furthermore, PET has a considerably higher radiation dose compared with skeletal scintigraphy, while MRI has the advantage of conferring no ionising radiation. The effective dose of FDG PET/CT has been reported to range from 13.5–32.2 mSv, a consideration particularly in paediatric patients as survival rates improve [30, 31]. In addition, PET has been reported to show a relatively high number of false-positive lesions which require follow-up [7]. PET remains less accessible and more expensive than WB-MRI and bone scintigraphy. PET/MRI is now also clinically available and has been utilised in the setting of paediatric malignancy, a particular advantage being the total lack of ionising radiation [32–34].

However, its role in the skeletal staging of ES is yet to be established.

The current study has several limitations. The WB-MRI and scintigraphic diagnosis of skeletal metastases were based on the identification of typical imaging appearances [13], which is in keeping with clinical practice where biopsy is only performed in indeterminate cases, such as illustrated in Fig. 3. Therefore, in the absence of a histological 'gold standard', sensitivity and specificity could not be determined for either technique. Due to the retrospective nature of the study, there was no standard protocol. Ideally, all WB-MRI and bone scintigraphy studies should have been performed on the same day using identical techniques, thus allowing the most accurate comparison between modalities. We had to rely on the assessment of external bone scans in 23.7% of cases, but they were all considered to be of diagnostic quality. Regarding time delay between studies, 57.7% were performed on the same day and 90.1% within 7 days of each other, so it is not felt that this significantly influenced the results. Due to the 12-year retrospective nature of the study, it would never have been possible to use state-of-the-art equipment or the most up-to-date sequences, but the length of the study was required to allow as many patients to be included considering the rarity of the tumour. It is possible that newer WB-MRI sequences such as whole-body diffusion-weighted imaging, WB-Dixon sequences and possibly the use of contrast may be more sensitive than basic T1W SE and STIR sequences [9, 35]. It is also likely that the use of SPECT-CT would have increased the sensitivity of the detection of skeletal metastases [11], but this would be at the cost of a significant increase in radiation dose which is undesirable in a predominantly paediatric/adolescent population. The overall number of metastases was low, but consistent with the reported literature. Clinical and imaging follow-up of skeletal metastases including treatment response was not assessed, but this was not an aim of the study.

Scintigraphy was better than WB-MRI for the identification of skull metastases, but in no case was an isolated skull metastasis identified. Skull vault metastases from ES are relatively rare (3.8% in the current study), with only a few cases reported in the literature [6, 10, 36, 37]. However, in all previously reported cases, the skull metastasis was either clinically evident or associated with other metastases. Therefore, the possibility of an isolated occult skull vault metastasis being missed on WB-MRI would be extremely unlikely.

The implications for the identification of skeletal metastases in terms of treatment modification and prognosis are well recognised [38, 39]. The current study has identified a 7% increase in the demonstration of skeletal metastases on WB-MRI compared with bone scintigraphy in a large group of patients with primary ES of bone. Future studies comparing WB-MRI with FDG PET would be required to determine whether the difference in the detection of skeletal metastases would justify the increased radiation dose and cost of FDG PET.

## Conclusion

WB-MRI is more sensitive than bone scintigraphy in detecting skeletal metastases in ES of bone and can safely replace bone scintigraphy for staging of the skeleton, with the acknowledgement of the possibility of missing a clinically occult skull vault metastasis.

**Funding** The authors state that this work has not received any funding.

## Compliance with ethical standards

**Guarantor** The scientific guarantor of this publication is Dr. Asif Saifuddin.

**Conflict of interest** The authors of this manuscript declare no relationships with any companies, whose products or services may be related to the subject matter of the article.

**Statistics and biometry** No complex statistical methods were necessary for this paper.

**Informed consent** Written informed consent was waived by the Institutional Review Board.

**Ethical approval** Institutional Review Board approval was obtained.

**Methodology**
- retrospective
- diagnostic study
- performed at one institution

## References

1. Arndt CAS, Rose PS, Folpe AL, Laack NN (2012) Common musculoskeletal tumors of childhood and adolescence. Mayo Clin Proc 87:475–487
2. Gorlick R, Janeway K, Lessnick S, Randall RL, Marina N (2013) Children's oncology group's 2013 blueprint for research: bone tumors. Pediatr Blood Cancer 60:1009–1015
3. Murphey MD, Senchak LT, Mambalam PK et al (2013) From the radiologic pathology archives: Ewing sarcoma family of tumors: radiologic-pathologic correlation. Radiographics 33:803–831
4. Gerrand C, Athanasou N, Brennan B et al (2016) UK guidelines for the management of bone sarcomas. Clin Sarcoma Res 6:7
5. Casali PG, Bielack S, Abecassis N et al (2018) Bone sarcomas: ESMO-PaedCan-EURACAN Clinical Practice Guidelines for diagnosis, treatment and follow-up. Ann Oncol 29:iv79–iv95
6. Hattori T, Yamakawa H, Nakayama N et al (1999) Skull metastasis of Ewing's sarcoma–three case reports. Neurol Med Chir (Tokyo) 39:946–949
7. Daldrup-Link HE, Franzius C, Link TM et al (2001) Whole-body MR imaging for detection of bone metastases in children and young adults: comparison with skeletal scintigraphy and FDG PET. AJR Am J Roentgenol 177:229–236
8. Kumar J, Seith A, Kumar A et al (2008) Whole-body MR imaging with the use of parallel imaging for detection of skeletal metastases in pediatric patients with small-cell neoplasms: comparison with skeletal scintigraphy and FDG PET/CT. Pediatr Radiol 38:953–962

9. Costelloe CM, Madewell JE, Kundra V, Harrell RK, Bassett RL Jr, Ma J (2013) Conspicuity of bone metastases on fast Dixon-based multisequence whole-body MRI: clinical utility per sequence. Magn Reson Imaging 31:669–675
10. Rana K, Wadhwa V, Bhargava EK, Batra V, Mandal S (2015) Ewing's sarcoma multifocal metastases to temporal and occipital bone: a rare presentation. J Clin Diagn Res 9:MD04–MD05
11. Rager O, Nkoulou R, Exquis N et al (2017) Whole-body SPECT/CT versus planar bone scan with targeted SPECT/CT for metastatic workup. Biomed Res Int 2017:7039406–7039408
12. Vanel D (2004) MRI of bone metastases: the choice of the sequence. Cancer Imaging 4:30–35
13. O'Sullivan GJ, Carty FL, Cronin CG (2015) Imaging of bone metastasis: an update. World J Radiol 7:202–211
14. Vanel D, Casadei R, Alberghini M, Razgallah M, Busacca M, Albisinni U (2009) MR imaging of bone metastases and choice of sequence: spin echo, in-phase gradient echo, diffusion, and contrast medium. Semin Musculoskelet Radiol 13:97–103
15. Cotterill SJ, Ahrens S, Paulussen M et al (2000) Prognostic factors in Ewing's tumor of bone: analysis of 975 patients from the European Intergroup Cooperative Ewing's Sarcoma Study Group. J Clin Oncol 18:3108–3114
16. Hargaden G, O'Connell M, Kavanagh E, Powell T, Ward R, Eustace S (2003) Current concepts in whole-body imaging using turbo short tau inversion recovery MR imaging. AJR Am J Roentgenol 180: 247–252
17. Smets AM, Deurloo EE, Slager TJE, Stoker J, Bipat S (2018) Whole-body magnetic resonance imaging for detection of skeletal metastases in children and young people with primary solid tumors - systematic review. Pediatr Radiol 48:241–252
18. Eustace S, Tello R, DeCarvalho V et al (1997) A comparison of whole-body turboSTIR MR imaging and planar 99mTc-methylene diphosphonate scintigraphy in the examination of patients with suspected skeletal metastases. AJR Am J Roentgenol 169:1655–1661
19. Gosfield E 3rd, Alavi A, Kneeland B (1993) Comparison of radionuclide bone scans and magnetic resonance imaging in detecting spinal metastases. J Nucl Med 34:2191–2198
20. Avrahami E, Tadmor R, Dally O, Hadar H (1989) Early MR demonstration of spinal metastases in patients with normal radiographs and CT and radionuclide bone scans. J Comput Assist Tomogr 13: 598–602
21. Flickinger FW, Sanal SM (1994) Bone marrow MRI: techniques and accuracy for detecting breast cancer metastases. Magn Reson Imaging 12:829–835
22. Siegel MJ, Acharyya S, Hoffer FA et al (2013) Whole-body MR imaging for staging of malignant tumors in pediatric patients: results of the American College of Radiology Imaging Network 6660 Trial. Radiology 266:599–609
23. Goo HW, Choi SH, Ghim T, Moon HN, Seo JJ (2005) Whole-body MRI of paediatric malignant tumours: comparison with conventional oncological imaging methods. Pediatr Radiol 35:766–773
24. Mazumdar A, Siegel MJ, Narra V, Luchtman-Jones L (2002) Whole-body fast inversion recovery MR imaging of small cell neoplasms in pediatric patients: a pilot study. AJR Am J Roentgenol 179:1261–1266
25. Kellenberger CJ, Miller SF, Khan M, Gilday DL, Weitzman S, Babyn PS (2004) Initial experience with FSE STIR whole-body MR imaging for staging lymphoma in children. Eur Radiol 14: 1829–1841
26. Quartuccio N, Fox J, Kuk D et al (2015) Pediatric bone sarcoma: diagnostic performance of $^{18}$F-FDG PET/CT versus conventional imaging for initial staging and follow-up. AJR Am J Roentgenol 204:153–160
27. Ulaner GA, Magnan H, Healey JH, Weber WA, Meyers PA (2014) Is methylene diphosphonate bone scan necessary for initial staging of Ewing sarcoma if 18F-FDG PET/CT is performed? AJR Am J Roentgenol 202:859–867
28. London K, Stege C, Cross S et al (2012) 18F-FDG PET/CT compared to conventional imaging modalities in pediatric primary bone tumors. Pediatr Radiol 42:418–430
29. Palmerini E, Colangeli M, Nanni C et al (2017) The role of FDG PET/CT in patients treated with neoadjuvant chemotherapy for localized bone sarcomas. Eur J Nucl Med Mol Imaging 44:215–223
30. Huang B, Law MW, Khong PL (2009) Whole-body PET/CT scanning: estimation of radiation dose and cancer risk. Radiology 251: 166–174
31. Willowson KP, Bailey EA, Bailey DL (2012) A retrospective evaluation of radiation dose associated with low dose FDG protocols in whole-body PET/CT. Australas Phys Eng Sci Med 35:49–53
32. Purz S, Sabri O, Viehweger A et al (2014) Potential pediatric applications of PET/MR. J Nucl Med 55:32S–39S
33. Daldrup-Link H (2017) How PET/MR can add value for children with cancer. Curr Radiol Rep 5:15–39
34. Lee YZ, Oldan JD, Fordham LA (2017) Pediatric applications of hybrid PET/MR imaging. Magn Reson Imaging Clin N Am 25: 367–375
35. Stecco A, Trisoglio A, Soligo E, Berardo S, Sukhovei L, Carriero A (2018) Whole-body MRI with diffusion-weighted imaging in bone metastases: a narrative review. Diagnostics (Basel) 8:45–56
36. Puerta P, Guillén A, Mora J, Suñol M, Ferrer E (2015) Isolated skull metastasis of Ewing's sarcoma in a child. Austin J Cancer Clin Res 2:1–3
37. Asif N, Khan AQ, Siddiqui YS, Mustafa H (2010) Metastasis from scapular Ewing's sarcoma presenting as sutural diastasis: an unusual presentation. Int J Shoulder Surg 4:18–21
38. Biswas B, Bakhshi S (2016) Management of Ewing sarcoma family of tumors: current scenario and unmet need. World J Orthop 7:527–538
39. Ozaki T (2015) Diagnosis and treatment of Ewing sarcoma of the bone: a review article. J Orthop Sci 20:250–263